



**Improvements in Modeling Thermospheric Densities
Using New EUV and FUV Solar Indices**

**Bruce R. Bowman
W. Kent Tobiska**

**16th AAS/AIAA Space Flight
Mechanics Conference**

Tampa, Florida

January 22-26, 2006

AAS Publications Office, P.O. Box 28130, San Diego, CA 92198

Improvements in Modeling Thermospheric Densities Using New EUV and FUV Solar Indices

Bruce R. Bowman*
Air Force Space Command
Space Analysis Division/XPY
bruce.bowman@peterson.af.mil
719-556-3710

W. Kent Tobiska
Space Environment Technologies
ktobiska@spacenvironment.net
310-573-4185

Major improvements in empirical thermospheric density modeling using new solar irradiance indices are reported. The development of a new solar extreme ultraviolet (EUV) irradiance index and a new far ultraviolet (FUV) Schumann-Runge Continuum (SRC) index are described. The far ultraviolet SRC energy, which has a unit optical depth in the lower thermosphere, has historically not been included in Jacchia and MSIS type models. The SRC is the main source of thermospheric molecular oxygen dissociation from photoabsorption. The standard solar extreme ultraviolet (EUV) irradiance F_{10} proxy alone has been used in these types of models although the energy in the SRC contributes to lower thermospheric heating, and subsequently, density changes in higher layers. We show major improvements in satellite drag modeling by incorporating a new EUV index derived from SOHO data, and a new SRC index derived from UARS and SORCE observations. We describe the formation of the new solar indices, S_{EUV} and E_{SRC} , that quantifies energy in EUV (26-34 nm) and FUV (145-165 nm), and report on their use for improving thermospheric density specifications.

Introduction

Density model errors on the order of 15%-20% one standard deviation have been recognized for all empirical models¹ developed since the mid 1960s. These large density

* This paper is declared a work of the US Government and is not subject to copyright protection in the US DOD Distribution A. Approved for public release; distribution unlimited.

standard deviations corresponding to maximum density errors of 40-60% as observed in satellite drag data. There are two main reasons for these consistently large values. One is the result of not modeling the semiannual density variation² as a function of solar activity, and the other results from not modeling the full thermospheric heating from solar ultraviolet radiation. Geomagnetic storms provide episodic, and overall smaller, contributions to the standard deviation. The semiannual density variations, based on solar activity, have been previously addressed². However, the complete ultraviolet effects on the thermosphere have not previously been analyzed. All previous empirical atmospheric models³⁻⁶ have used the F_{10} and 81-day average \overline{F}_{10} proxies as representative of the solar ultraviolet (UV) heating. However, the unmodeled errors derived from satellite drag data, as displayed in Figure 1 for 1999, all show very large density errors with approximately 27-day periods, representing one solar rotation cycle. These errors are the result of not fully modeling the ultraviolet radiation effects on the thermosphere, which have a one solar rotation periodicity. The purpose of this paper is to characterize the ultraviolet heating using new solar indices covering the wavelength range from the extreme to mid ultraviolet region.

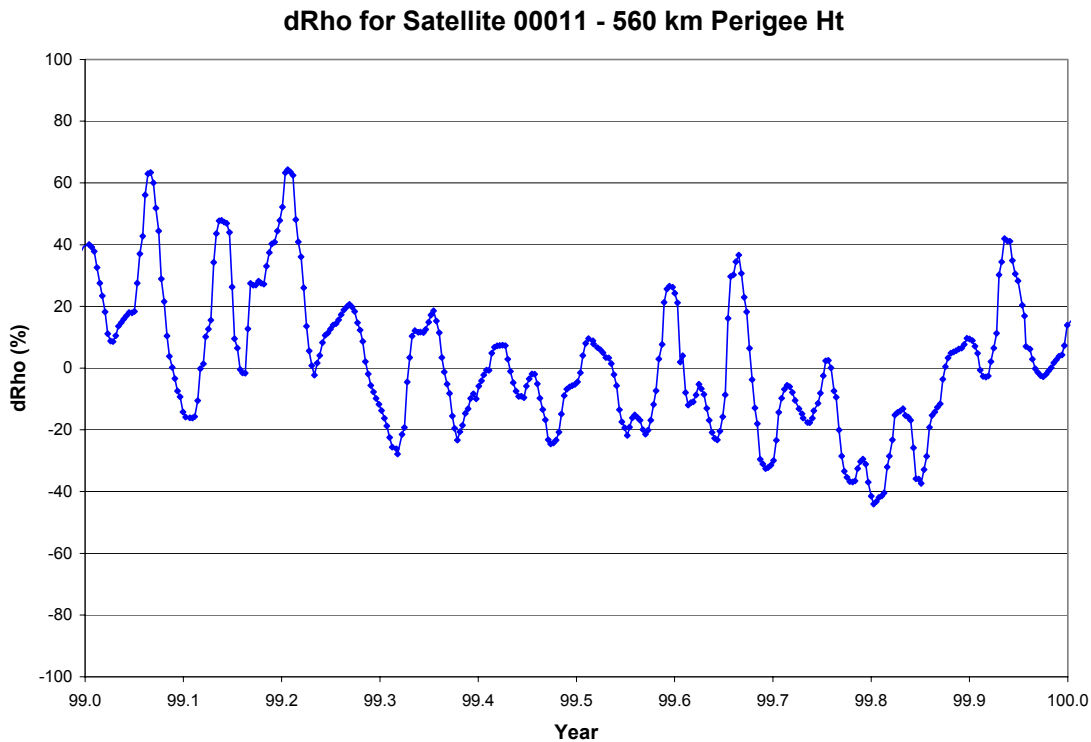


Figure 1. Density errors, $dRho$, from Jacchia 70^3 during 1999 from analysis of the ballistic coefficient (B) values obtained from the orbit decay of the spherical satellite 00011 with a perigee height of 560 km.

Figure 2 is a plot of the altitude at which the maximum absorption rate of solar UV radiation occurs as a function of wavelength⁷. The solar index F_{10} is really a proxy index because it is measured at a 10.7-cm wavelength (off the scale below), which is not a direct measure of any ultraviolet radiation. It has always been assumed that this proxy is a good, although imperfect, measure of the EUV heating. However, recently real

ultraviolet heating indices have been developed that represent the extreme (EUV), far (FUV), and mid (MUV) solar UV radiation. Figure 2 below suggests that besides an EUV index, that is required, an FUV, and possible an MUV index needs to be considered to capture all the potential UV heating of the thermosphere.

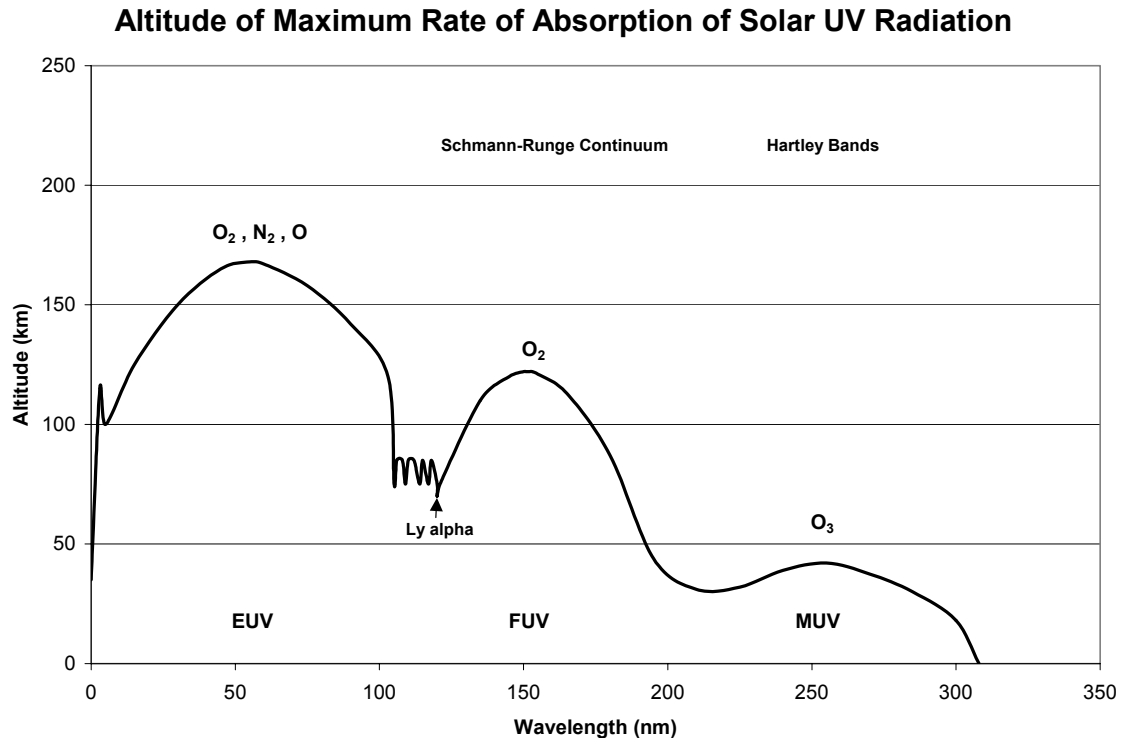


Figure 2. The altitude of the maximum rate of absorption of solar ultraviolet radiation as a function of solar spectrum wavelength. EUV - extreme ultraviolet, FUV - far ultraviolet, and MUV - mid ultraviolet region. The relevant atomic/molecular species for absorption is also listed.

Solar Indices

We have developed and studied a variety of solar indices in order to characterize the solar energy absorbed in the atmosphere that leads to density changes observed by satellites. We use the evolving terms *solar proxy* and *solar index* as described by ISO 21348⁸ to indicate measured or modeled data used a) as substitutes for solar spectral irradiances at different wavelengths or integrated bandpasses (*solar proxy*) and b) as indicators, often of levels of activity, for solar irradiances at specific wavelengths or integrated bandpasses (*solar index*). Table 1 summarizes these solar indices for atmospheric heating, their ISO 21348 spectral category, sub-category, wavelength range in units of nm, solar source temperature region, solar source feature, altitude region of terrestrial atmosphere absorption at unit optical depth in units of km, and terrestrial atmosphere thermal region of energy absorption. The indices marked with an asterisk (*) are those that have been selected for use in a modified Jacchia atmospheric density model that is described later in this paper. Spectral subcategory abbreviations are used for soft X-ray (XUV), extreme

ultraviolet (EUV), far ultraviolet (FUV), middle ultraviolet (MUV), and ultraviolet (UV) solar emissions.

Index	ISO 21348 Spectral category	ISO 21348 Spectral sub-category	Wavelength range (nm)	Solar source temperature region	Solar source feature	Atmosphere absorption (unit optical depth, km)	Atmosphere absorption (thermal region)
X _{b10}	X-rays	X-rays	0.1-0.8	Corona	Active region fibrils	70-90	Mesosphere
E ₁₀	X-rays and ultraviolet	XUV+EUV	1-105	Chromosphere, corona	Active region plage, network	90-500	Thermosphere
*F ₁₀	Radio	Radio	10.7E7	Transition region, cool corona	Active region	90-500	Thermosphere
*S _{EUV}	UV	EUV	26-34	Chromosphere, corona	Active region, plage, network	200-300	Thermosphere
XL ₁₀	X-rays and UV	X-rays+H Lyman- α	0.1-0.8,121	Chromosphere, transition region, corona	Active region fibrils + plage, network	70-90	Mesosphere
H Ly α	UV	H Lyman- α	121	Transition region, chromosphere	Active region, plage, network	70-90	Mesosphere
E _{SRC}	UV	FUV	145-165	Photosphere, chromosphere	Plage and network	125	Lower thermosphere
*Mg ₁₀	UV	MUV	280	Chromosphere	Active region	20	Stratosphere
E _{HRT}	UV	MUV	245-254	Photosphere	Granules	25	Stratosphere

*Used in the modified Jacchia model exospheric temperature equation described in this paper.

Table 1. Solar indices for atmospheric heating.

Index	Observing facility	Instrument	Observation time frame	Measurement cadence	Measurement latency	Operational availability
F ₁₀	Penticton ground observatory	Radio telescope	1947-2005	3 times/day	Up to 24 hours	yes
S _{EUV}	SOHO	SEM	1996-2005	15-second	Up to 24 hours	(a)
XL ₁₀	GOES-12, UARS, SORCE, TIMED	XRS, SOLSTICE (2), SEE	1991-2005	1-minute, 16 times/day	Up to 10 minutes, up to 48 hours	(b)
E _{SRC}	UARS, SORCE	SOLSTICE (2)	1991-2005	16 times/day	Up to 48 hours	(c)
Mg ₁₀	NOAA-16,17	SBUV	1991-2005	2 times/day	Up to 24 hours	yes
E _{HRT}	UARS, SORCE	SOLSTICE (2)	1991-2005	16 times/day	Up to 48 hours	(c)

(a) SOHO is a NASA research satellite but provides daily irradiances on an operational measurement cadence.

(b) GOES XRS is a NOAA operational instrument whereas TIMED/SEE and SORCE/SOLSTICE are NASA research satellites providing daily irradiances on an operational measurement cadence.

(c) UARS/SOLSTICE is no longer active; SORCE/SOLSTICE is intended to provide data for several years.

Table 2. Characteristics of daily reported solar indices.

Table 2 summarizes the characteristics of the subset of daily reported solar indices used in this work. The index name, its observing facility, the instrument used to observe the solar emission, the observation set time frame, the measurement cadence, the data latency, and the operational availability of each index are also listed.

The daily indices considered in this study are described, including their source, development, and formulation. They include F₁₀, S_{EUV}, Mg₁₀, XL₁₀, E_{SRC}, and E_{HRT}. We report our solar indices over the common time frame of January 1, 1996 through June 12, 2005 since each of them exists during this period. After development and validation, these indices were used as inputs into an atmospheric density model (described below) and the resulting densities were compared with satellite-derived density data. As a result of analyzing the residual error between the modeled and satellite-derived densities, only the F₁₀, S_{EUV}, and Mg₁₀ indices, along with their 81-day centered smoothed values, were selected for use in the final atmospheric density model formulation (discussion below).

F₁₀: The 10.7-cm solar radio flux, F_{10} , was first observed⁹ on a daily basis starting February 14, 1947 and is now produced daily by the Canadian National Research Council's Herzberg Institute of Astrophysics at its ground-based Dominion Radio Astrophysical Observatory located in Penticton, British Columbia. Observations of the F_{10} flux density values are made at 18, 20 and 22 UT each day¹⁰. The 20 UT values are archived at the World Data Center and used for this study. The physical units of F_{10} are $1 \times 10^{-22} \text{ W m}^{-2} \text{ Hz}^{-1}$ and we use the numerical value without the multiplier as is customarily done and expressed as solar flux units (sfu). In other words, a 10.7-cm radio emission of $150 \times 10^{-22} \text{ W m}^{-2} \text{ Hz}^{-1}$ is simply referred to as $F_{10} = 150 \text{ sfu}$.

We have created a running 81-day centered smoothed set of values using the moving box-car method and these data are referred to as either F_{81} or \bar{F}_{10} . In our analysis, we have used linear regression with daily F_{10} to scale and report all other solar indices in units of sfu. Missing data values are not included in the regressions.

F_{10} is the traditional solar energy proxy that has been used since Jacchia developed empirical exospheric temperature equations for atmospheric density models³⁻⁵. It's formation is physically dominated by non-thermal processes in the solar transition region and cool corona and, while it is a non-effective solar emission relative to the Earth's atmosphere, it is a useful proxy for the broad combination of chromospheric, transition region, and coronal solar EUV emissions modulated by bright solar active regions whose energy, at Earth, is deposited in the thermosphere.

S_{EUV}: The NASA/ESA Solar and Heliospheric Observatory (SOHO) research satellite operates in a halo orbit at the Lagrange Point 1 (L1) on the Earth-Sun line, approximately 1.5 million km from the Earth, and has an uninterrupted view of the Sun. One of the instruments on SOHO is the Solar Extreme-ultraviolet Monitor (SEM) that was built and is operated by University of Southern California's (USC) Space Science Center (SSC). SOHO was launched on December 2, 1995 and SEM has been making observations since December 16, 1995. As part of its continuous solar observations, the SEM instrument measures the 26–34 nm solar EUV emission with 15-second time resolution in its first order broadband wavelength range. The orbit and solar data are both retrieved daily by USC SSC for processing in order to create daily solar irradiances with a latency of up to 24 hours¹¹.

We have used the integrated 26–34 nm emission (SOHO_SEM_{26-34}) and normalized it by dividing the daily value by the common time frame mean value. The mean value, $\text{SOHO_SEM}_{26-34\text{mean}}$, is $1.99328\text{e}+10 \text{ photons cm}^{-2} \text{ s}^{-1}$. The normalized value is converted to sfu through linear regression with F_{10} over the common time frame and the resulting index is called S_{EUV} . Equation 1 provides the formulation used to derive S_{EUV} .

$$S_{\text{EUV}} = (-23.47) + (149.90) \times (\text{SOHO_SEM}_{26-34} / \text{SOHO_SEM}_{26-34\text{mean}}) \quad (1)$$

The broadband (wavelength integrated) SEM 26-34 nm irradiances, represented by the S_{EUV} index, are EUV line emissions dominated by the chromospheric He II line at 30.4 nm with contributions from other chromospheric and coronal lines. This energy principally comes from solar active regions, plage, and network. Once the photons reach the Earth, they are deposited (absorbed) in the terrestrial thermosphere mostly by atomic oxygen above 200 km.

E_{SRC}: The solar FUV Schumann-Runge Continuum (SRC) contains emission between 125–175 nm from the photosphere and lower chromosphere. This solar energy is deposited in the terrestrial mesosphere and lower thermosphere (80–125 km) primarily through the energy released from the dissociation of molecular oxygen.

The SRC has been observed by the SOLSTICE instrument on the UARS¹² and SORCE¹³ NASA research satellites as well as by the SEE instrument on NASA TIMED research satellite¹⁴. We have selected the 145–165 nm band as a representative wavelength range of the SRC since the emission in this band is mostly deposited in the 110–125 km altitude region. For our analysis, we have integrated the daily SOLSTICE 145–165 nm emission and created a normalized value by dividing the daily value by the common time frame mean value, SOLSTICE_{145-165-mean}, which has a value of 2.1104972e+11 photons cm⁻² s⁻¹. Next, we performed a linear regression with F₁₀ to report the index E_{SRC}, in sfu, as shown in equation 2.

$$E_{\text{SRC}} = (-784.03) + (909.34) \times (\text{SOLSTICE}_{145-165} / \text{SOLSTICE}_{145-165\text{-mean}}) \quad (2)$$

E_{HRT}: The solar MUV Hartley Band (HB) contains emission between 245–254 nm from the photosphere. This solar energy is deposited in the terrestrial stratosphere (30–40 km) primarily through the energy released from the dissociation of ozone. The HB has been observed by the SOLSTICE instrument on the UARS and SORCE NASA research satellites. For our analysis, we have integrated the daily SOLSTICE 245–254 nm emission and created a normalized value by dividing the daily value by the common time frame mean value, SOLSTICE_{245-254-mean}, which has a value of 3.1496268e+13 photons cm⁻² s⁻¹. Next, we performed a linear regression with F₁₀ to report the index E_{HRT}, in sfu, as shown in equation 3.

$$E_{\text{HRT}} = (-726.27) + (851.57) \times \text{HB}_{245-254} / \text{HB}_{245-254\text{-mean}} \quad (3)$$

Mg₁₀: The NOAA series operational satellites, e.g., NOAA 16 and NOAA 17, host the Solar Backscatter Ultraviolet (SBUV) spectrometer that has the objective of monitoring ozone in the Earth’s lower atmosphere. In its discrete operating mode, a diffuser screen is placed in front of the instrument’s aperture in order to scatter solar MUV radiation near 280 nm into the instrument.

This solar spectral region contains both photospheric continuum and chromospheric line emissions. The chromospheric Mg II *h* and *k* lines at 279.56 and 280.27 nm, respectively, and the weakly varying photospheric wings or continuum longward and shortward of the core line emission, are operationally observed by the instrument. The Mg II core-to-wing ratio (cwr) is calculated between the variable lines and nearly non-varying wings. The result is a measure of chromospheric and some photospheric solar active region activity independent of instrument sensitivity change through time, and is referred to as the Mg II cwr, which is provided daily by NOAA Space Environment Center (SEC)¹⁵.

The ratio is an especially good proxy for some solar FUV and EUV emissions. We have taken the Mg II cwr and performed a linear regression with F₁₀ for the common time frame to derive the Mg₁₀ index that is the Mg II cwr reported in sfu units. Equation 4 provides the calculation of Mg₁₀ based on the NOAA 16 SBUV Mg II cwr data.

$$\text{Mg}_{10} = (-1943.85) + (7606.56) \times \text{Mg_II}_{\text{NOAA16}} \quad (4)$$

XL₁₀: The X-ray Spectrometer (XRS) instrument is part of the instrument package on the GOES series operational spacecraft. The XRS on GOES 10 and GOES 12 provide the 0.1–0.8 nm solar X-ray emission with 1-minute cadence and 5-minute latency. These data are continuously reported by NOAA SEC¹⁶.

X-rays in the 0.1–0.8 nm range come from the cool and hot corona and are typically a combination of both very bright solar active region background that varies slowly (days to months) plus flares that vary rapidly (minutes to hours), respectively. The photons arriving at Earth are primarily absorbed in the mesosphere and lower thermosphere (80–90 km) by molecular oxygen and nitrogen where they ionize those neutral constituents to create the ionospheric D-region.

An index of the solar X-ray active region background, without the flare component, has been developed for operational use¹⁷. This is called the X_{b10} index and is used to represent the daily energy that is deposited into the mesosphere and lower thermosphere.

The 0.1-0.8 nm X-rays are a major energy source in these atmospheric regions during high solar activity but relinquish their dominance to the competing hydrogen (H) Lyman-alpha (Lya) emission during moderate and low solar activity. Lya is also deposited in the same atmospheric regions, is created in the solar upper chromosphere and transition region, and demarcates the EUV from the FUV spectral regions. It is formed primarily in solar active regions, plage, and network; the photons, arriving at Earth, are absorbed in the mesosphere and lower thermosphere where they dissociate nitric oxide (NO) and participate in water (H₂O) chemistry. Lya has been observed by the SOLSTICE instrument on the UARS and SORCE NASA research satellites as well as by the SEE instrument on NASA TIMED research satellite¹⁸.

Since these two solar emissions are competing drivers of the mesosphere and lower thermosphere, we have developed a mixed solar index of the X_{b10} and Lya. It is weighted to reflect mostly X_{b10} during solar maximum and to reflect mostly Lya during moderate and low solar activity. The independent, normalized F₈₁ (81-day centered smoothed F₁₀ divided by the common time frame mean value, i.e., F_{81-normalized}) is used as the weighting function and multiplied with the X_{b10} and Lya as fractions to their solar maximum values. Equation 5 provides the XL₁₀ index reported in sfu.

$$XL_{10} = \{F_{81\text{-normalized}} \times (X_{b10}/X_{b10\text{-max}}) + (1 - F_{81\text{-normalized}}) \times (Lya/Lya_{\text{max}})\} \times F_{81} \quad (5)$$

Figure 3 below shows a plot of the F₁₀, S_{EUUV}, E_{SRC}, and Mg₁₀ indices for a period during 2001. Even though all indices demonstrate a 27-day solar rotation period there appears to be significant variability in amplitude and phase between the indices that warrants testing of all the different indices in determining new temperature/density equations.

Solar Flux Indices - 2001

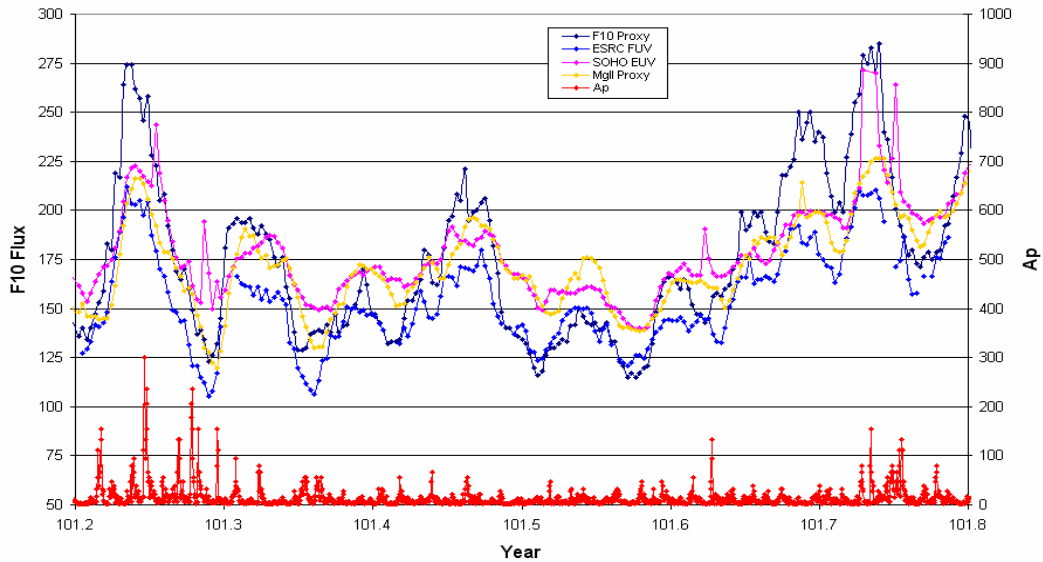


Figure 3. Solar flux values for the F_{10} proxy, the S_{EUV} index, the E_{SRC} index, and the Mg_{10} proxy, are shown for a 2001 year time period. The 3-hour a_p values are also plotted. All solar flux are in sfu.

Exospheric Temperature Analysis

The density data used for the analysis is very accurate daily density values¹⁹ obtained from satellites at perigee altitudes of 175 km to 1000 km. Table 3 lists these satellites with corresponding dates and perigee altitudes. Most of the satellites are approximately spherical in shape, with the remainder being cylindrical that have been determined to have no frontal area problems which would produce inaccurate density values.

Ht (km)	1996-99	2000-04	Type	Shape				
175		26692	PAM-D	Spheriod				
		25935	PAM-D	Spheriod				
200	22781	22781	PAM-D	Spheriod				
	06073	06073	Venus Lander	Spheriod				
250	22277	22277	PAM-D	Spheriod	Red	Low i	<35 deg	
	04053	04053	IntelSat 3	Cylinder	Yellow	Mid i	~50 deg	
300	14694	14694	R/B	Cylinder	Green	Crit i	~63 deg	
	08063	08063	R/B	Cylinder	Blue	High i	>70 deg	
350	02150	02150	OV3-1	Cylinder				
	02389	02389	OV3-3	Cylinder				
400	12388	12388	RadarCal	Sphere				
	14483	14483	RadarCal	Sphere				
	04382	04382	DFH-1	~Sphere				
500	00011	00011	Vanguard 2	Sphere				
600	00047	00047	R/B	Cylinder				
700								
800	02909	02909	Calsphere	Sphere				
	02826	02826	Calsphere	Sphere				
1000	00900	00900	Calsphere	Sphere				

Table 3. The satellites used for the analysis. The perigee heights and available data spans are listed for each satellite. The orbit inclinations (i) are color-coded.

The daily values start in 1996 to correspond to the start of the S_{EUV} index values. The RMS of the daily values is 2-4 %¹⁹.

The density values were converted into daily Tc temperature values using the Jacchia 70 empirical atmospheric density model³. To obtain accurate Tc values other large unmodeled density variations, besides the solar Tc variations, must be removed. A major density variation, aside from the 11-year and 27-day solar heating effect, is the semiannual change. This can be as large as 250% from a July minimum to an October maximum during solar maximum years, and as small as 60% from July to October during solar minimum years (at 600 km)². Jacchia³⁻⁵ only partially modeled this variation by considering it as a constant in amplitude (as a function of height) and phase from year to year regardless of solar conditions. However, Jacchia did state that the semiannual variation has an amplitude that depends on solar activity, although the correlation has never been measured. To correct this incomplete modeling the semiannual variation was computed on a yearly basis from previously derived density data². Jacchia's 70 model equation was then replaced using these observed semiannual yearly variations. A smaller correction to Jacchia's model was also made for the observed errors in the latitude and local solar time density variations. From these different model corrections an accurate Tc value, due almost entirely to solar heating, was obtained. The observed daily density value was used through iterating on Tc until the input observed density value was matched to the output density (using the iterated Tc value) to less than 1%.

Temperature Fits

The initial Tc temperature equation used for the new model was

$$Tc = a_0 + a_1 \bar{F}_{10} + a_2 \Delta F_{10} + a_3 \Delta S_{EUV} + a_4 \Delta E_{SRC} \quad (6)$$

The \bar{F}_{10} represents the 81-day centered average value of the F_{10} index. The delta values (ΔF_{10} , ΔS_{EUV} , ΔE_{SRC}) represent the difference of the daily and 81-day centered average value of the index. The 81-day (3 solar rotation period) centered index was initially used because of the studies conducted by Jacchia³⁻⁵ in determining the best number of solar rotation periods to use for averaging. However, a 2 and 4 solar rotation period were also tested for use in computing the centered indices. This is discussed below.

A linear least squares solution was obtained for the a_i coefficients in equation (6). Table 4 lists the RMS and coefficient values obtained for different combinations of terms. To avoid possible Tc altitude dependencies it was decided to initially use only the data from the 4 satellites around 400 km perigee altitude. The data from 1996 through 2004 was used, with the exception of the 2002 data when no E_{SRC} index values were available. Also, to avoid increases in Tc due to geomagnetic storms all daily data with $a_p > 25$ were rejected. This meant that if an index required a lag time of 5 days, each of the 5 days prior to the current time had to have $a_p < 25$ for the current daily density data to be used.

1996-2004, excluding 2002					
Trial	RMS	dF ₁₀	dS _{EUV}	dE _{SRC}	dMg ₁₀
Run	(dTc deg)				
1	19.9	1.405			
2	17.4	0.552			1.405
3	15.7	0.606		0.918	0.691
4	14.8	0.172	2.604		
5	14.7		2.835		
6	14.7		2.542		0.241
7	14.3		2.299	0.564	
8	14.1	0.255	1.914	0.615	
Lag (days)		1	1	5	1

Table 4. The coefficients and RMS values obtained from the least squares fits of Tc are shown. The terms used in each fit are given by a non-zero coefficient value in °K/sfu. The lag time used for each coefficient is also included. The dF₁₀, dS_{EUV}, dE_{SRC}, and dMg₁₀ values correspond to the ΔF₁₀, ΔS_{EUV}, ΔE_{SRC}, and ΔMg₁₀ described in the text.

Table 4 lists the results of some of the least squares fits that were obtained from this data. Approximately 4600 daily density points were finally used in the solution based on data from these 4 satellites from 1996 through 2004. The first fit consisted of using just \bar{F}_{10} and F₁₀, the standard solar indices used in the Jacchia models. The large RMS value of 19.9° indicates that the equation still has large unmodeled errors in Tc. The second fit listed in Table 4 adds the Mg₁₀ index to the equation. Since the F₁₀ values have always been assigned a 1-day lag the Mg₁₀ index was also assigned a 1-day lag for the fit. This was based on the assumption that the F₁₀ and Mg₁₀ index represented the heating of the thermosphere in the extreme ultraviolet region. The addition of the Mg₁₀ index to the F₁₀ equation provided a definite improvement to the Tc fit. In adding the Schumann-Runge index it was not know what the lag should be, but because the maximum heating occurred 50 km below the altitude of maximum EUV heating it was anticipated that the lag would be longer because of the additional time required for the heat transport to higher altitudes. Other fits in determining the E_{SRC} lag time, described below, show a 5-day value as the best to use for this index. Therefore, the fits listed in Table 4 using the E_{SRC} index use this 5-day lag. For the EUV effect a lag of 1 day was kept for the S_{EUV} index.

Adding the Mg₁₀ index reduced the RMS value by more than 2°. Another approximately 2° reduction in the RMS resulted from adding the E_{SRC} index to the Tc equations. Table 4 shows the RMS results for different combinations of terms used. Since all the indices are in sfu the magnitudes of the coefficients show the relative significance of each index. The S_{EUV} index is by far the largest contributor to the Tc solar heating variation. The contribution of the F₁₀ index becomes much smaller as EUV and FUV indices are used, indicating that in the original Jacchia equations the F₁₀ index was only approximating the real EUV heating effect. The real EUV heating index S_{EUV}, based on the 26-34 nm data, better represents the EUV heating in the thermosphere. The next most significant index is the E_{SRC} index, which contributes approximately one-third of the density variation of the EUV heating, and over twice the effect of the heating variation from the F₁₀ index, which represents the effect from the solar cool corona. As a final observation the Mg₁₀

index does not appear to be significant when the S_{EUV} index is present. However, as will be discussed later, this is a result of using too short a lag time for the Mg_{10} index.

Table 5 lists the analysis on the lag time of the S_{EUV} index, and then the E_{SRC} index. As was expected the 1-day value is the best to use for representing the EUV heating. Table 5 also shows the analysis of the E_{SRC} lag times. The RMS values appear to level out at the 5-day lag time, with no significant improvement beyond this value. Therefore, a 5-day value was assigned for this index lag time.

1996-2004, excluding 2002		
	S_{EUV} Runs	E_{SRC} Runs
Lag	RMS	RMS
(days)	dTc (deg)	dTc (deg)
1	14.1	-----
2	14.2	14.8
3	14.9	14.6
4	15.7	14.3
5	16.4	14.2
6	16.8	14.1
7	-----	14.1
8	-----	14.2
9	-----	14.3

Table 5. The RMS values are listed for the Tc fit based on varying lag times for first the ΔS_{EUV} coefficient, and then the ΔE_{SRC} coefficient. For the S_{EUV} runs the lag time of 1 day was used for F_{10} and 5 days for E_{SRC} . For the E_{SRC} runs a lag time of 1 day was used for both F_{10} and S_{EUV} . The highlighted RMS values indicate the best lag time fit selected for the indices.

11-Year Cycle Temperature Fits

It was also decided to verify Jacchia's results of the best average time used for the \bar{F}_{10} index. Table 6 lists the results of using 2, 3, and 4 solar rotation centered periods for the long-term averages of F_{10} , S_{EUV} , E_{SRC} , and Mg_{10} indices. Use of the 3-solar rotation period produces the best RMS average, thus confirming the results previously obtained by Jacchia³⁻⁵.

Table 6 also lists the results of using 81-day centered values of either F_{10} , S_{EUV} , or Mg_{10} for the representation of the long-term 11-year solar cycle variation (the a_l term in equation (6)). The customary index in use for all previous models has been \bar{F}_{10} . For this analysis the 81-day centered S_{EUV} , and then the Mg_{10} , values were used to replace the \bar{F}_{10} value for the long-term effects. The \bar{F}_{10} value is significantly better than using either of the other long-term indices. This is surprising since using the long term S_{EUV} was expected to produce very similar results as with using the EUV \bar{F}_{10} proxy. At present it is unclear why the \bar{F}_{10} proxy performs so much better than the other two indices.

Run	RMS (dTc deg)	Average
1	20.2	54-day centered
2	19.7	81-day centered
3	21.5	108-day centered
		81-day centered
4	19.7	F ₁₀
5	30.5	S _{EUUV}
6	41.6	Mg ₁₀

Table 6. The RMS values are listed for the Tc fits based on using 54-day, 81-day, and 108-day centered average values for F₁₀, S_{EUUV}, and E_{SRC}. Also listed are the RMS results using F₁₀, S_{EUUV}, or Mg₁₀ 81-day centered averages for the 11-year solar variability.

Temperature Height Variations

The next step in the analysis was to determine any altitude dependency on Tc. Many Tc least squares fits were obtained using data from groups of satellites at different perigee altitudes. The fits were done using all the terms in equation (6). Figure 4 is a plot of the resulting coefficient values as a function of altitude. Since all the coefficients are in units of sfu the total dTc/Flux is plotted as the sum of the coefficient values for different altitudes. The plot shows that the S_{EUUV} index has the largest contribution to the temperature variation (65% of the total dTc at 400 km), with the E_{SRC} having the next largest contribution (23% at 400 km). The F₁₀ variation, though much smaller (only 12%), is still significant enough to include in the overall Tc variation. There is a small but statistically significant height dependency for all the coefficients. However, when all the data for all the satellites were fit, and an additional height term was included for the S_{EUUV} index, the result was the same (to less than 1%) as not including the height dependent term. Therefore, it was decided that a height term was not required for the Tc equation.

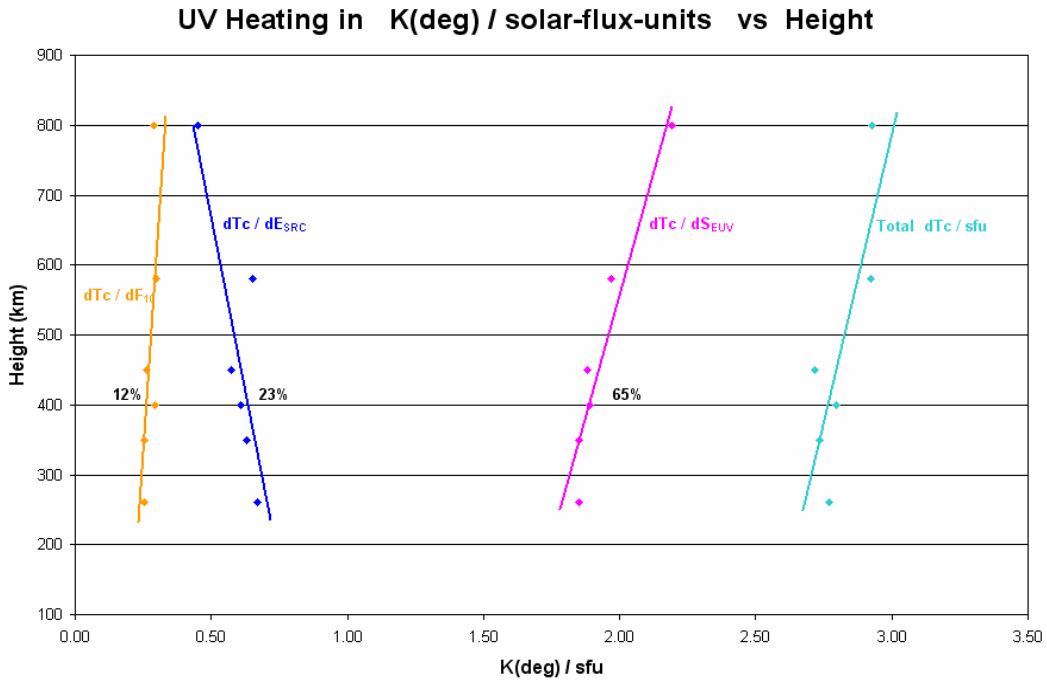


Figure 4. Plots of the fitted coefficient values ($^{\circ}\text{K}/\text{sfu}$) are shown as a function of altitude. The total dTc/flux values are also plotted. The percentage of the total contribution of each coefficient is listed for an altitude of 400 km.

Mg₁₀ Analysis

The Mg₁₀ index was used as an addition to the EUV index, as shown in Table 4. The results, using a 1-day lag, showed that the Mg₁₀ contribution was insignificant compared to the S_{EUV} contribution. However, if the lag time is wrong for Mg₁₀ then the 1-day lag results for Mg₁₀ could be much worse than for the real case. It was decided to substitute the Mg₁₀ index for the E_{SRC} index, and run fits with various lag times for Mg₁₀. Table 7 shows the surprising results of the test. The best fit corresponds to a 5-day lag time, the same as for the E_{SRC} index.

Mg₁₀ Lag Test:	
Lag (days)	RMS dTc (deg)
2	14.5
3	14.3
4	14.3
5	14.1
6	14.2
E_{SRC} correlation: 0.85	

Table 7. The RMS value is listed for the Tc fit based on varying lag times for the ΔMg_{10} coefficient. The highlighted RMS value indicates the best lag time fit selected for the Mg₁₀ use.

The coefficient for the Mg_{10} index, using the 5-day lag, is approximately $0.4^\circ/\text{flux}$, which is close to the magnitude of the E_{SRC} coefficient. When Mg_{10} , with a 5-day lag, is used in addition to E_{SRC} the correlation is 0.85 between the Mg_{10} and E_{SRC} index. These results indicate that the Mg_{10} index represents the FUV, and not EUV, effects in the thermosphere. The Mg_{10} index appears to be a good substitute for the E_{SRC} index. To verify using Mg_{10} in place of E_{SRC} new Tc equations, first using E_{SRC} and then Mg_{10} , were fit using F_{10} and S_{EUV} with data from all satellites. The new Tc equations were then placed into the Jacchia model, along with the observed yearly semiannual variations, to compute new B values for satellite 12388 at 400 km perigee altitude. The B values were then compared to the true B (BAve) computed as a long-term average value²⁰. Figure 5 shows the results of the year 2000 orbit fits using first the E_{SRC} index and then the Mg_{10} index.

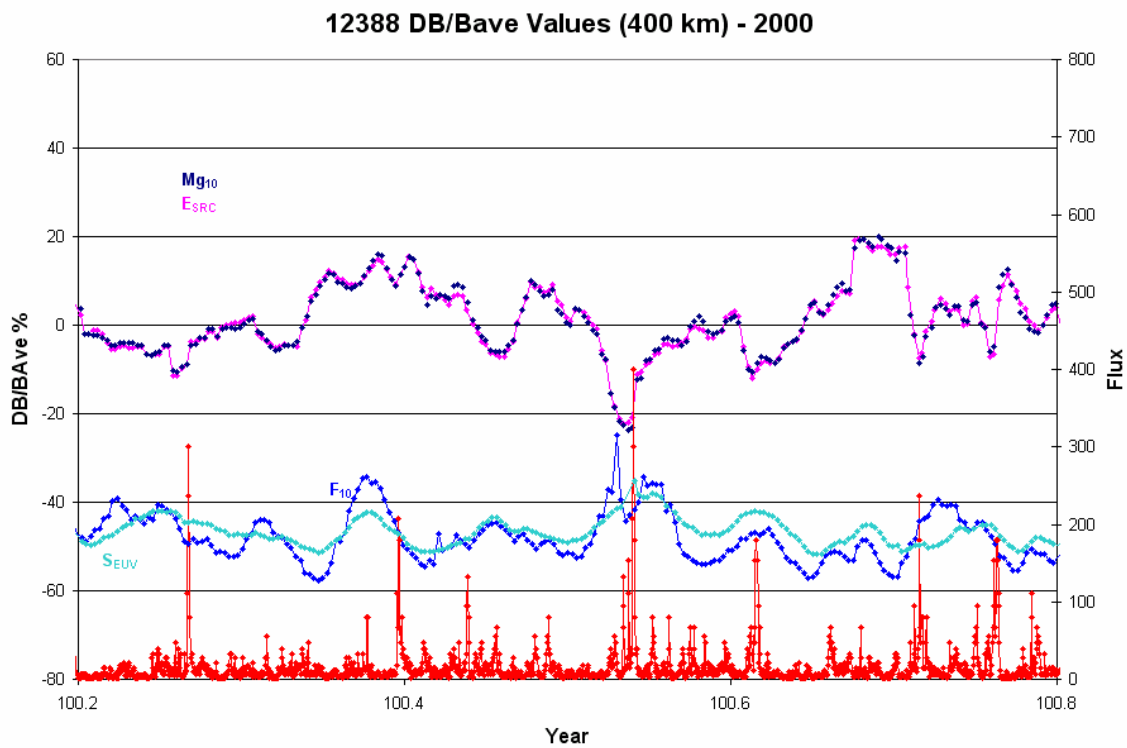


Figure 5. The delta B variations obtained from the differential orbit correction for satellite 12388 during a year 2000 time period are shown. The DB variations (B-BAve), using first the E_{SRC} coefficient, and then the Mg_{10} coefficient, in the Tc fitted equation are plotted. The F_{10} , S_{EUV} , and a_p indices plots are included.

The B values were computed for 1999 and 2000 time periods. DB values were computed by differencing the daily values with the true B values. The differences between the use of the different indices are almost insignificant. These results confirm the supposition that the Mg_{10} index is an excellent representation for the FUV thermospheric heating effect, and an excellent replacement for the E_{SRC} index.

XL₁₀ and Hartley Band Analysis

The analysis was extended to include heating at altitudes below 100 km. The XL₁₀ index was used to represent maximum thermospheric heating at approximately 100 km, while the Hartley Band index was used for effects produced at 50 km altitude. Table 8 lists the results of the Tc least squares fits incorporating the XL₁₀ index. Since the Mg₁₀ index was substituted for the E_{SRC} index, solar index values were available for all of 2002. Therefore, the RMS values in Table 8 are slightly higher than listed in previous tables because of inclusion of the 2002 data. Lag times of 2 through 9 days were used, with the best fit occurring at a lag time of 8 days. The best improvement was small, only 0.3° in Tc, but not insignificant. These results confirm the supposition that the lower the maximum altitude of absorption the smaller the effect and the longer the lag time for propagating the effects to higher altitudes. Since this effect had a very small temperature/density effect on the upper thermosphere it was decided not to include it in the final new Tc equation.

The results of the Hartley Band index showed no correlation of the index with Tc variations. Thus, the 50 km height is too low for any significant propagation to much higher altitudes.

XL ₁₀ Lag Test: (All 1996-2004)					
Lag (days)	RMS dTc (deg)	dF ₁₀	dS _{EUUV}	dMg ₁₀	dXL ₁₀
-----	15.27	X	X	X	
2	15.22	X	X	X	X
3	15.18	X	X	X	X
4	15.11	X	X	X	X
5	15.07	X	X	X	X
6	15.03	X	X	X	X
7	15.01	X	X	X	X
8	14.99	X	X	X	X
9	15.11	X	X	X	X
8	15.14	X	X		X

Table 8. The RMS value is listed for the Tc fit based on varying lag times for the ΔXL₁₀ coefficient. The X values indicate which coefficients were used in the fit. The highlighted RMS value indicates the best lag time fit selected for the XL₁₀ use.

Density Comparisons

The solution of the best Tc equation was finally obtained using all the satellites for all the years from 1996 through 2004. The resulting equation, from Table 9 below, is:

$$Tc = 379.0 + 3.353 \bar{F}_{10} + 0.358 \Delta F_{10} + 2.094 \Delta S_{EUUV} + 0.343 \Delta M_{g10} \quad (7)$$

To determine the accuracy of the coefficients it was decided to refit the equation numerous times by removing data from different combinations of a solar maximum plus

a solar minimum year. Table 9 lists the results, with the first entry being the results of the complete fit with no data removed. The final entry is the RMS values of the coefficients based on the sample of 12 different fits computed.

RMS (dTc deg)	Const	F_{10B}	dF₁₀	dS_{EUV}	dMg₁₀	Sol Min Yr Removed	Sol Max Yr Removed
19.7	379.0	3.353	0.358	2.094	0.343	None	None
19.8	377.1	3.362	0.456	1.894	0.356	1996	1999
19.6	376.2	3.371	0.391	1.987	0.412	1996	2000
19.3	380.5	3.336	0.311	2.132	0.380	1996	2001
19.4	375.1	3.383	0.426	1.889	0.452	1996	2002
19.8	378.1	3.357	0.458	1.917	0.362	1997	1999
19.6	377.3	3.364	0.394	2.010	0.419	1997	2000
19.3	381.2	3.332	0.314	2.151	0.387	1997	2001
19.5	376.2	3.377	0.429	1.910	0.458	1997	2002
20.0	378.2	3.358	0.386	1.996	0.390	1998	2003
20.5	377.2	3.361	0.437	1.904	0.359	2004	1999
20.3	376.6	3.367	0.367	2.000	0.420	2004	2000
20.1	379.9	3.338	0.276	2.162	0.378	2004	2001
RMS:	1.9	0.016	0.060	0.102	0.035		

Table 9. The RMS values are listed for the Tc fits with a solar maximum and a solar minimum year removed. All the data (1996-2004) for all the satellites were used in the Tc fits. The RMS values for the coefficients are also listed. All coefficient values are in °K/sfu.

The final testing was done by placing the new Tc equation (7) in the Jacchia 70 atmospheric model, along with the observed yearly semiannual variations, to produce the JBH05 model. This was then used to compute new DB variations for satellite 12388 at 400 km perigee altitude. Figures 6 and 7 show the results of the recomputed DB variations for years 1999 and 2000. Both figures show a marked improvement in reducing the DB variations with respect to the 27-day solar rotation period. There still appears to be a slight correlation of the DB variation with the solar period when using the new Tc equation (JBH05 model), but the amplitude has been greatly reduced from using the original Jacchia 70 model. The resulting density standard deviations, using the new Tc equation to fit this satellite's data during 1999 and 2000, for 1) the original Jacchia 70 model, 2) Jacchia 70 using the yearly observed semiannual variation, and 3) the JBH05 model are 16.3%, 11.8%, and 8.1% respectively. This shows that the observed yearly semiannual variation and the new solar indice equation each contributes approximately 50% of the total improvement at this height of 400 km. Further analysis will be done in the future using different satellites, time periods, and heights to quantify the overall density improvements using the new Tc equation.

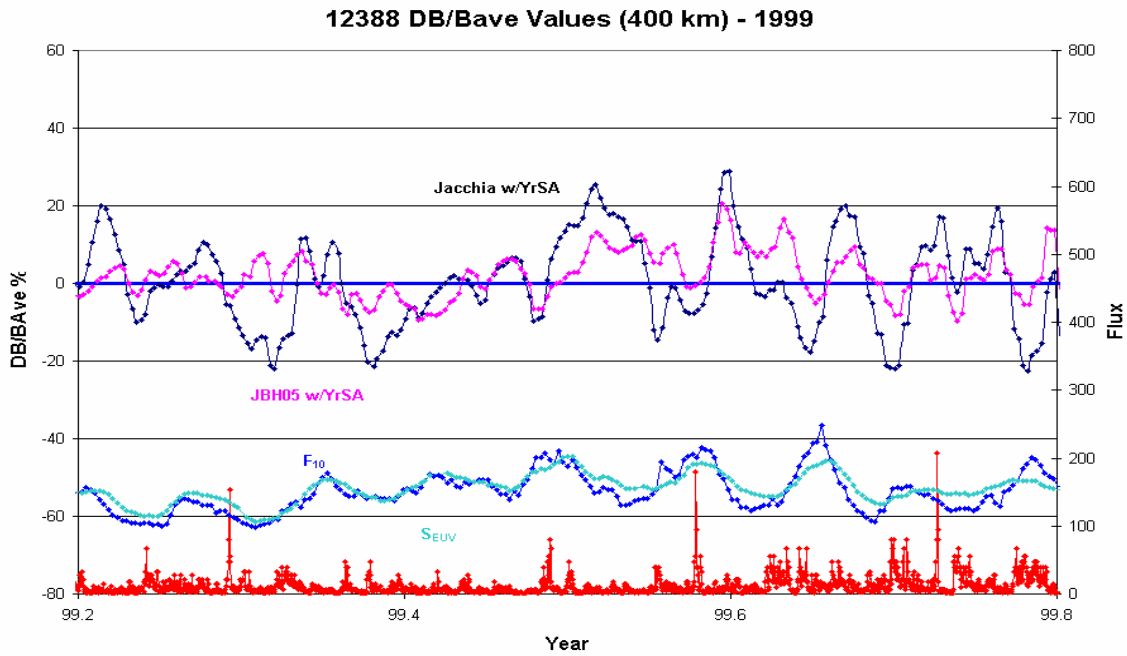


Figure 6. The delta B variations are listed for satellite 12388 for a year 1999 time period. The Jacchia data is based on orbit corrections using the original Jacchia 70 model with the observed 1999 semiannual applied. The JBH05 data uses the new complete T_c equation (7) with the observed 1999 semiannual variation also applied. The indices F_{10} , S_{EUV} , and a_p are also plotted.

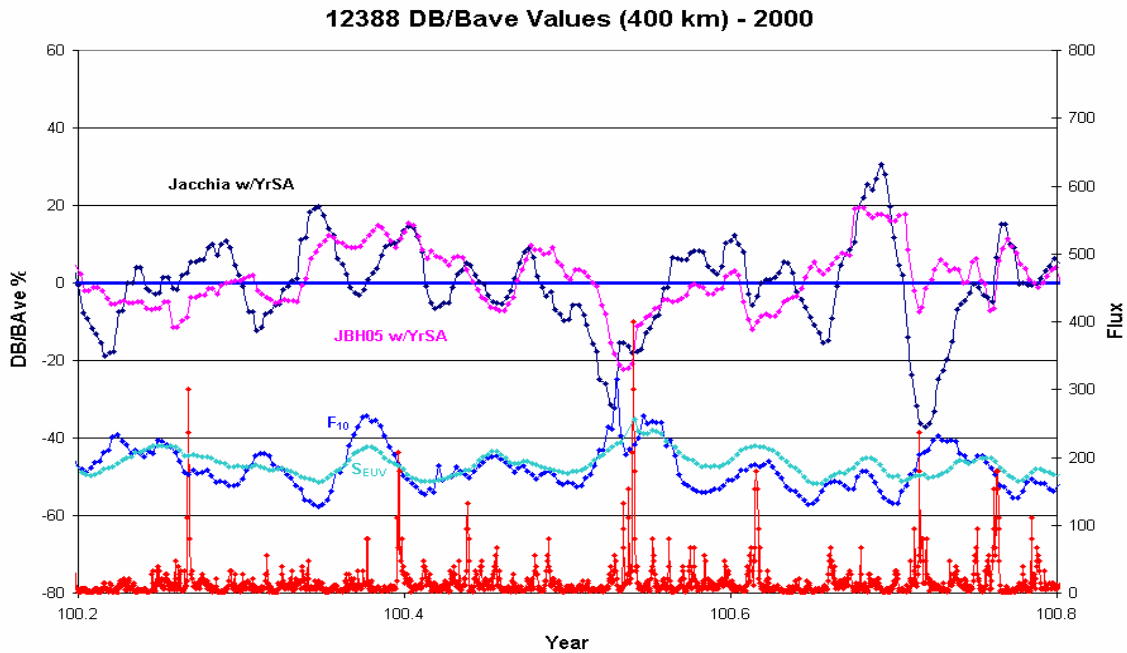


Figure 7. The delta B variations are listed for satellite 12388 for a year 2000 time period. The Jacchia data is based on orbit corrections using the original Jacchia 70 model with the observed 2000 semiannual applied. The JBH05 data uses the new complete T_c equation (7) with the observed 2000 semiannual variation also applied. The indices F_{10} , S_{EUV} , and a_p are also plotted.

Conclusions

Three interesting conclusions can be drawn from this work regarding the physics of solar energy input into the terrestrial upper atmosphere. These new insights are related to the atmospheric response to solar photons and the inertial characteristics of the atmosphere.

First, the improvement in empirical density modeling using the new EUV S_{EUV} radiation and FUV Schumann-Runge Continuum emission for the energy input into the lower thermosphere suggests that a missing solar energy component is one reason an uncertainty plateau of $\sim 15\%$ (at 400 km) 1-sigma density error was never reduced by the Jacchia and MSIS type models which incorporated only the F_{10} EUV emission proxy.

Second, the significant improvement in empirical density modeling using three solar source region proxies or indices, i.e., F_{10} (broadband proxy for transition region, cool corona EUV), S_{EUV} (index for chromospheric EUV), and Mg_{10} (SRC proxy for photospheric, lower chromospheric FUV), suggests that the atmosphere response can be better modeled with individual solar source region emissions than with a total integrated irradiance index such as E_{10} ²¹. While numerous studies over the past several years have been conducted using F_{10} and E_{10} to determine if the latter provides improved atmospheric densities, the results have always been ambiguous. The approach in this work of separating the solar source region emissions has demonstrated a clear improvement on the use of either F_{10} or E_{10} individually as the sole solar energy input.

Third, the very good fits between the model density and satellite-derived density data suggests that there may be bounding conditions on the time constants for the vertical transport component of the kinetic processes of molecular diffusion, eddy mixing, and turbulent mixing, respectively. The model density in this work was tested by solar energy input into four regions, i.e., the middle thermosphere above 200 km (F_{10} and S_{EUV}), lower thermosphere around 125 km (E_{SRC} and Mg_{10}), the upper mesosphere around 80 km (XL_{10}), and the stratosphere around 40 km (E_{HRT}).

As external solar energy pulses are deposited into the middle thermosphere, temperature, pressure, and concentration gradients are formed and this sets up the conditions for diffusion. Since atomic oxygen is the principal species of the middle thermosphere, its diffusion velocity must be on the order of a day corresponding to the best fits of 1-day lags for F_{10} and S_{EUV} . For the lower thermosphere, where the molecular nitrogen dominates the neutral atmosphere and eddy mixing is the principal kinetic process, the molecular flow's diffusion velocity may be on the order of 5 days based on the best fit of a 5-day lag for E_{SRC} and Mg_{10} .

For the upper mesosphere, where the molecular nitrogen dominates the neutral atmosphere and turbulent mixing is the principal kinetic process, analysis of the XL_{10} proxy for the X-ray and Lyman-alpha wavelengths suggests that the molecular flow's vertical transport velocity may be on the order of 8 days corresponding to the best fit of a 8-day lag for XL_{10} .

For the stratosphere, where the molecular nitrogen dominates the neutral atmosphere and turbulent mixing is the principal kinetic process, the E_{HRT} proxy for the Hartley Band MUV wavelengths used multiple-day lags and none were found to have a significant

impact on the thermospheric densities. In this case, nothing can be said about the molecular flow's vertical transport velocity in this analysis.

Finally, preliminary analysis using the new solar indices indicates that the density standard deviation reduction at 400 km is on the order of 25%, with another 25% reduction occurring when using the yearly observed semiannual variation.

Acknowledgments

The authors thank Jeff Forbes, Tim Fuller-Rowell, Stan Solomon, and Geoff Crowley for their insights into the physics and dynamics of the terrestrial upper atmosphere. The UARS SOLSTICE, TIMED SEE, and SORCE SOLSTICE PI teams, and especially Tom Woods and Chris Pankratz, made this study possible with their gracious provision of XUV, EUV, FUV, and MUV satellite data. The SOHO SEM PI team, and especially Darrell Judge and Andrew Jones, made an invaluable contribution through their provision of the SEM first order data. We thank Dave Bower of Space Environment Technologies for his long-hours of programming to make numerous data sets available in common formats. The authors also thank the NASA LWS Focused Science Team led by Art Richmond for their generous incorporation of the results of this work into their broad program of studying the thermosphere and ionosphere. Finally, we want to thank Mr. Frank A. Marcos of the Air Force Research Laboratory for his valuable suggestions.

References

1. Marcos, F.A., "Accuracy of Atmospheric Drag Models at Low Satellite Altitudes," *Advances in Space Research*, **10**, p 417, 1990.
2. Bowman, B.R., "The Semiannual Thermospheric Density Variation From 1970 to 2002 Between 200-1100km," AAS 2004-174, *AAS/AIAA Spaceflight Mechanics Meeting*, Maui, HI, February, 2004.
3. Jacchia, L.G., New Static Models of the Thermosphere and Exosphere with Empirical Temperature Profiles, *Smithson. Astrophys. Special Report 313*, 1970.
4. Jacchia, L.G., Revised Static Models of the Thermosphere and Exosphere with Empirical Temperature Profiles, *Smithson. Astrophys. Special Report 332*, 1971.
5. Jacchia, L.G., Thermospheric Temperature, Density, and Composition: New Models, *Smithson. Astrophys. Special Report 375*, 1977.
6. Hedin, A. E.; "Extension of the MSIS Thermosphere Model into the Middle and Lower Atmosphere," *J. Geophys. Res.*, **96**, pp. 1159-1172, 1991.
7. Jursa, A. S., Handbook of Geophysics and the Space Environment, Air Force Geophysics Laboratory, Air Force Systems Command, pp 2-1 to 2-21, 1985.
8. "Space Environment (natural and artificial) - Process for Determining Solar Irradiances," ISO International Standard (IS) 21348, International Standards Organization, Geneva, in press, 2006.
9. Covington, A.E., Solar noise observations on 10.7 centimeters, *Proc. of the I.R.E.*, **36**, 454, 1948.
10. http://hia-ihp.nrc-cnrc.gc.ca/drao/icarus_e.html
11. Judge, D.L., H.S. Ogawa, D.R. McMullin, P. Gangopadhyay, and J.M. Pap, "The SOHO CELIAS/SEM EUV Database from SC23 Minimum to the Present," *Adv. Space Res.*, **29** (12), 1963, 2001.

12. Rottman, G.J. and T.N. Woods, "The UARS SOLSTICE," *SPIE Proc.*, **2266**, 317, 1994.
13. McClintock, W.E., G.J. Rottman, and T.N. Woods, "SOLar Stellar Irradiance Comparison Experiment II (SOLSTICE II) for the NASA Earth Observing System's Solar Radiation and Climate Experiment Mission," *SPIE Proc.*, **4135**, 225, 2000.
14. Woods, T.N., G.J. Rottman, R.G. Roble, O.R. White, S.C. Solomon, G.M. Lawrence, J. Lean, and W.K. Tobiska, "TIMED Solar EUV Experiment," *SPIE Proc.*, **2266**, 467, 1994.
15. Viereck, R., L. Puga, D. McMullin, D. Judge, M. Weber, W.K. Tobiska, "The Mg II Index: A Proxy for Solar EUV," *Geophys. Res. Lett.*, **28** (7), 1342, 2001.
16. <http://www.sec.noaa.gov/>
17. Tobiska, W.K. and S.D. Bouwer, Solar flare evolution model for operational users, *IES2005 Proc.*, ed. J.M. Goodman, in press, 2005.
18. Woods, T.N., W.K. Tobiska, G.J. Rottman, and J.R. Worden, Improved solar Lyman α irradiance modeling from 1947 through 1999 based on UARS observations, *J. Geophys. Res.*, **105**, 27195, 2000.
19. Bowman, B.R., etc., "A Method for Computing Accurate Daily Atmospheric Density Values from Satellite Drag Data," AAS 2004-179, *AAS/AIAA Spaceflight Mechanics Meeting*, Maui, HI, February, 2004.
20. Bowman, B. R., "True Satellite Ballistic Coefficient Determination for HASDM," AIAA-2002-4887, *AIAA/AAS Astrodynamics Specialist Conference*, Monterey, California, August, 2002.
21. Tobiska, W.K., "Validating the Solar EUV Proxy, E10.7," *J. Geophys. Res.*, **106**, A12, 29969-29978, 2001.